JACS
JOURNAL OF THE AMERICAN CHEMICAL SOCIETY
pubs.acs.org/JACS
Article

Defective Nature of CdSe Quantum Dots Embedded in Inorganic Matrices

Wenke Li, Kai Li, Xiujian Zhao, Chao Liu,* and François-Xavier Coudert*

Cite This: J. Am. Chem. Soc. 2022, 144, 11296−11305
Read Online
ACCESS | Metrics & More | Article Recommendations | Supporting Information

ABSTRACT: Quantum dots (QDs) embedded in inorganic matrices have been extensively studied for their potential applications in lighting, displays, and solar cells. While a significant amount of research studies focused on their experimental fabrication, the origin of their relatively low photoluminescence quantum yield has not been investigated yet, although it severely hinders practical applications. In this study, we use time-dependent density functional theory (TDDFT) to pinpoint the nature of excited states of CdSe QDs embedded in various inorganic matrices. The formation of undercoordinated Se atoms and nonbridging oxygen atoms at the QD/glass interface is responsible for the localization of a hole wave function, leading to the formation of low-energy excited states with weak oscillator strength. These states provide pathways for nonradiative processes and compete with radiative emission. The photoluminescence performance is predicted for CdSe QDs in different matrices and validated by experiments. The results of this study have significant implications for understanding the underlying photophysics of CdSe QDs embedded in inorganic matrices that would facilitate the fabrication of highly luminescent glasses.

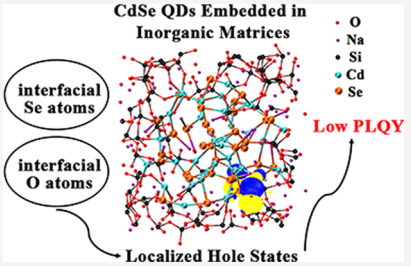

1. INTRODUCTION

Semiconductor quantum dots (QDs) were first realized experimentally in glasses[1] in 1981 and later as chemically synthesized colloidal nanocrystals[2] in 1983. QDs offer tunable photoluminescence (PL), high photoluminescence quantum yield (PLQY), and high color purity; thus, they have emerged as suitable materials for white light-emitting diodes (LEDs),[3] solar cells,[4] lasers,[5] etc. QDs feature a large surface-to-volume ratio and high surface energy, resulting in instability and degradation of emissive properties during storage and use. Therefore, large efforts have been made in the past decades to eliminate surface defects of colloidal QDs, for example, through surface passivation or by forming core−shell structures.[6−8] Although the PLQY of colloidal QDs can reach almost 100% after efficient passivation,[9,10] poor stability due to the introduction of organic ligands remains an important roadblock for their practical application.

Encapsulating QDs with an inorganic glass matrix can combine the excellent optical properties of QDs and the high chemical and thermal stability of the glass. Thus, QDs such as CdSe,[11−14] PbS,[15] and perovskite QDs[16−20] have been embedded in glasses and have attracted a lot of attention. However, the highest reported PLQYs for CdSe and $CsPbBr_3$ QDs embedded in glass matrices are 48.6%[21] and 86.9%,[18] respectively, which are much lower than their colloidal counterparts. The poor emissive properties of QDs embedded in glasses greatly hinder their commercial applications and the underlying mechanism has not been fully explored yet. However, it is experimentally challenging to probe the structural origin of the low PLQY of QDs due to the dense, insulating, and amorphous nature of the glass matrix and the dimensions of the QD/glass interface.

Instead, molecular simulations have proven to be a reliable approach to investigate the atomic and electronic structures of colloidal QDs. Atomistic modeling methods were used for the characterization of the ground state[22−25] and excited states[26−36] of CdSe QDs. These theoretical studies investigated the origin of defect emission of colloidal QDs and provide a better understanding of QDs' photophysics, giving guidance to the experimental design of novel materials, for example, using the passivation method. Indeed, while significant experimental efforts have been made in research on QDs in glass matrices, theoretical work based on the ab initio method is still scarce compared to that on colloidal QDs. The size-dependent band gap of QDs in different matrices has been studied based on the potential morphing method.[37] It was found that the confining potential depends exclusively on the nature of the matrix (and not on that of the dot). Furthermore, our previous study[38] suggested that the QDs could not maintain their ideal structure—even at their core—when they were incorporated into glass matrices, in stark contrast with colloidal QDs (which feature a slight rearrangement of surface atoms and maintain

Received: March 21, 2022
Published: June 17, 2022

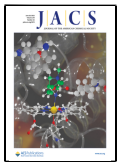

https://doi.org/10.1021/jacs.2c03039
J. Am. Chem. Soc. 2022, 144, 11296−11305

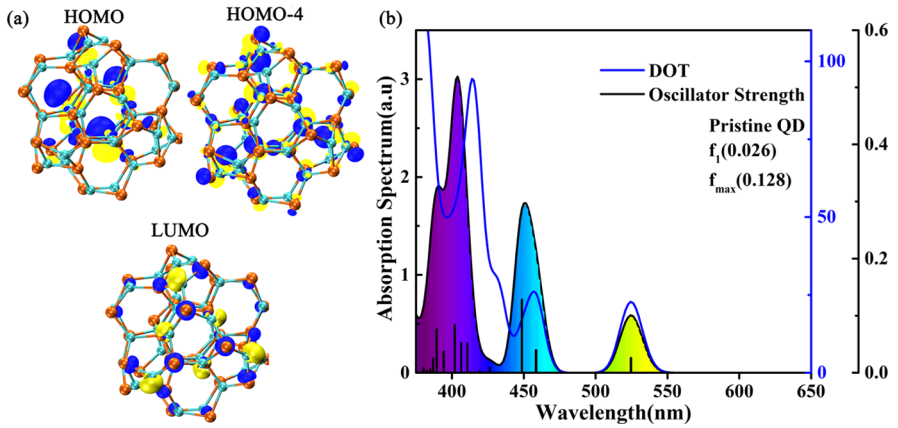

Figure 1. Molecular orbitals and absorption spectrum of a pristine $Cd_{33}Se_{33}$ QD. (a) The lowest-energy transition almost originates from HOMO to LUMO transitions with the oscillator strength equal to f_1. The excited state with the maximum oscillator strength (f_{max}) across 100 calculated transitions is mainly from HOMO-4 (low-lying occupied orbital (HOMO-n)) to LUMO. The color of the atoms in CdSe QDs is cyan for Cd and orange for Se. Blue and yellow regions denote positive and negative signs of wave functions, respectively. (b) Absorption spectrum (black line, shaded) and density of transitions (blue line). Black vertical bars show individual excited states, with the values for the oscillator strength shown at the right y-axis.

their bulk structure at the core). For CdSe QDs in binary alkali silicate glasses, the breakage of stable six-membered and four-membered Cd−Se rings was observed with the formation of Se−Na or Cd−O interfacial linkages. The unavoidable strong structural reconstruction contributes to the formation of undercoordinated surface atoms and nonbridging oxygen atoms at the QD/glass interface. These structural rearrangements are anticipated to exert a large effect on their electronic structure and the QD/glass interfacial structure, which might be the origin of low PLQY. Ground-state electronic calculations[39] confirmed this hypothesis, demonstrating that the nature of the highest occupied molecular orbitals (HOMOs) of CdSe QDs embedded in glass matrices was directly affected by the glass. The HOMO was determined by oxygen atoms in $(Na_2O)_{39}(SiO_2)_{78}(CdSe)_{33}$ glasses, while it was decided by Se atoms in other glass compositions based on the analysis of density of states. In addition, the disappearance of the pristine QD structure was verified by the atomic structure and band gap analysis. Consequently, the emission is not from the combination of defect emission and intrinsic emission of the pristine QD as commonly proposed. These studies exhibited the striking difference between QDs in colloidal solutions and in glass matrices, which we suggested to be the origin of the diverse luminescence performance. However, the nature of the transition (optically active or forbidden) from HOMO to lowest unoccupied molecular orbital (LUMO) could not be described by these ground-state electronic calculations, and therefore, the photophysics, especially the excited-state properties of CdSe QDs embedded in glass matrices, still needs to be investigated.

Here, we performed time-dependent density functional theory (TDDFT) calculations to present computational evidence that CdSe QDs embedded in inorganic matrices are defective in nature. The presence of the glass matrix inevitably contributes to significant structural reconstruction of the pristine QDs, resulting in the localization of the hole wave function on undercoordinated interfacial Se atoms and nonbridging oxygens. The small overlap between the localized hole and delocalized electron wave functions implies the weak oscillator strength of the first excited states, and therefore, poor emissive properties of those composites. The PLQYs of CdSe QDs embedded in glass samples that we fabricated are proportional to the oscillator strength of the lowest-energy transitions calculated. Our results reveal that the essentially unavoidable existence of undercoordinated Se atoms together with nonbridging oxygens at the QD/glass interface leads to a dense manifold of low-energy states, governing the emission properties of CdSe QDs in inorganic matrices. Our findings further provide the understanding of QDs embedded in glasses and could give guidance to design highly luminescent QDs embedded in glasses and colloidal QDs passivated by an inorganic shell.

2. RESULTS AND DISCUSSION

The fully relaxed structure of a pristine $Cd_{33}Se_{33}$ QD in vacuum, with 21 three-coordinated Se or Cd atoms on the surface and 12 four-coordinated Se or Cd atoms in the core, was generated by density functional theory (DFT) calculations, with the method used in our previous study (Figure 1a).[40] The nonlocal PBE0 hybrid exchange-correlation functional was employed, which has been proved to provide rather accurate geometry and excited-state description comparable to experimental findings based on extensive benchmarking tests on CdSe QDs[28,36,41]—for further details on how we generated the model and calculated the absorption spectra, see the Section 4. With our chosen methodology, the first absorption peak (Figure 1b) is located at 525 nm (2.36 eV), redshifted compared to the experimental value of 415 nm (~2.99 eV).[42] We do not intend to reproduce the exact value of the experimentally observed absorption peak but rather intend to probe the impact of inorganic matrices on a relative energy scale. Figure 1b also displays the density of transitions, which was obtained by applying Gaussian broadening to the calculated excitation energies. The high density of transitions with small oscillator strength indicates the optically forbidden states, as shown at higher energies (~425 nm) than the first absorption peak.

The HOMO to LUMO transition contributes to 98.58% of the lowest-energy transition with a weak oscillator strength equal to 0.026. In the pristine QD, the HOMO is found to be localized on the three-coordinated surface Se atom (Figure 1a), while the LUMO is delocalized due to the heavier effective mass of holes. The brightest peak with the highest oscillator strength (0.128) is

https://doi.org/10.1021/jacs.2c03039
J. Am. Chem. Soc. 2022, 144, 11296−11305

dominated by the HOMO-4 to LUMO transition. HOMO-4 is more delocalized than HOMO, resulting in the spatial overlap of electron and hole wave functions, leading to a significant absorption intensity.

Then, we incorporated the pristine QD into glass matrices of varying compositions, 25 Na_2O−75 SiO_2, 33Na_2O−67SiO_2, 20 Na_2O−5 CaO−75 SiO_2, and 15 Na_2O−10 CaO−75 SiO_2 (in mol%), serving as an initial structure for molecular dynamic (MD) simulations (Figure S1). These QDs embedded in glasses are labeled as Q25N75S, Q33N67S, Q20N5C75S, and Q15N10C75S (Table S1). The atomic structures of these glasses were generated by a combination of classical MD and ab initio MD (AIMD) simulations. Compared to the pristine QD, the final configuration (Figure 2) of the production run

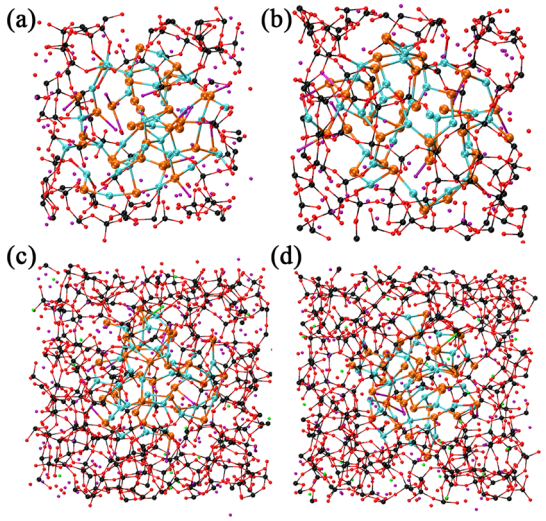

Figure 2. Final configuration of $Cd_{33}Se_{33}$ QDs embedded in different glasses taken from AIMD simulations. Glass composition: (a) 25 Na_2O−75 SiO_2−33 CdSe, (b) 33 Na_2O−67 SiO_2−33 CdSe, (c) 20 Na_2O−5 CaO−75 SiO_2−33 CdSe, and (d) 15 Na_2O−10 CaO−75 SiO_2−33 CdSe. The structure of a hybrid QD is distinctly different from that of a pristine QD, with a great ratio of undercoordinated surface atoms and breakage of stable $CdSe_4$ or Cd_4Se units even in the core (the structure of the hybrid QD is solely illustrated in Figure S2). The color of the atoms is as follows: Cd in cyan, Se in orange, O in red, Si in black, Na in purple, and Ca in green.

demonstrates significant reconstruction of the CdSe QD with breakage of the stable $CdSe_4$ or $SeCd_4$ units and formation of undercoordinated Cd or Se atoms at the interface (Figure S2). It was found that the two-coordinated surface Se atoms are responsible for the dark, surface-associated excitations, even in a stoichiometric CdSe QD with perfect ligand passivation.[36] Therefore, we hypothesize that the observed structural reconstruction will have a remarkable impact on the optical properties of CdSe QDs embedded in glasses compared to the pristine QD.

TDDFT calculations using the final configuration of each AIMD simulation exhibit distinct excited-state characteristics of CdSe QDs embedded in different glass matrices (Figure 3 and Table S2). The first immediate observation is that the first absorption peak is shifted compared with the pristine QD. The solvent effect has been extensively discussed in colloidal QDs experimentally and theoretically:[35,43−49] the relatively larger dielectric constant of semiconductor QDs compared to organic solutions gives rise to a dielectric confinement effect,[50,51] leading to the enhancement of exciton binding energy and oscillator strength. As a result, the first absorption peaks are often blueshifted for colloidal QDs in polar solutions. Although the glass matrices can be considered as a "polar solution" to some extent (Table S3), the shift of the first absorption peak does not have the same tendency as that in colloidal QDs. The dielectric constant of silicate glasses[52] is higher than that of CdSe QDs,[53] contributing to the disappearance of the dielectric confinement effect. Therefore, the blueshift of the first absorption peak was not observed in some of the surrounding glasses.

In addition, the oscillator strength of the lowest-energy transition ranges from 0.30 to 0.016 depending on the composition of glass matrices. In particular, the oscillator strength of the Q33N67S glass is much lower than that of other compositions (Figure 3b), which can be explained by the analysis of computed energy levels and charge density distribution of frontier orbitals.

The ground-state electronic structure calculation predicts that the HOMO of the Q33N67S glasses is mainly determined by the oxygen atoms in glass matrices (Figure 4), while the Se atoms play a dominate role in determining the HOMO for other compositions. Meanwhile, the LUMO of CdSe QDs embedded in glasses is decided by the Cd atoms. Therefore, the frontier orbitals are spatially separated in Q33N67S glasses, indicating little possibility of hole and electron recombination even if the HOMO to LUMO transition is optically active. The excited-state calculation further confirms this finding as the first excited-state transition is mainly derived from the HOMO to LUMO transition, which is optically active but with weak oscillator strength in Q33N67S glasses (Figure 3b).

The charge density distributions (depicted in Figures 5 and 6) are consistent with the computed energy levels. In Q25N75S glasses, the lowest-energy transition is mainly ascribed to the transition from HOMO (Figure 5a) to LUMO (Figure 5b), which is distributed on the undercoordinated surface atoms of the hybrid QD. It is worth mentioning that both orbitals are distributed on some interfacial oxygens, indicating the hybridized nature of frontier orbitals (see Figure S3 for details). The oscillator strength of the first excited states (also the brightest state with the maximum oscillator strength f_{max}) is enhanced compared to the pristine QD due to the improved overlap between the hole and electron wave functions. The absorption spectra and distribution of charge density of frontier orbitals are also calculated for some representative configurations from the production run of the AIMD simulation (Figure S4). It is clear that the multiple interactions between glass matrices and QDs lead to different atomic structures of the hybrid QD; hence, diverse excited states are observed for Q25N75S glasses. In some configurations, the first absorption peak is blueshifted (Figure S4c), rather than redshifted, compared with the pristine QD (Figure S4a,b). The oscillator strength of the first excited-state transition also slightly fluctuates and the charge density distribution exhibits similar features. All these observations point to a consistent result: the lowest-energy transition is optically active and the frontier orbitals are mainly distributed on the surface Se atoms.

However, in Q33N67S glasses, the HOMO is almost localized on the nonbridging oxygen atoms at the QD/glass interface (Figures 5c and S3c), while the LUMO is mostly delocalized on the hybrid QD (Figures 5d and S3d) with a small portion on nonbridging oxygen atoms. The small spatial overlap between the electron and hole wave functions indicates the weak oscillator strength of the lowest-energy transition. A weakly

https://doi.org/10.1021/jacs.2c03039
J. Am. Chem. Soc. 2022, 144, 11296−11305

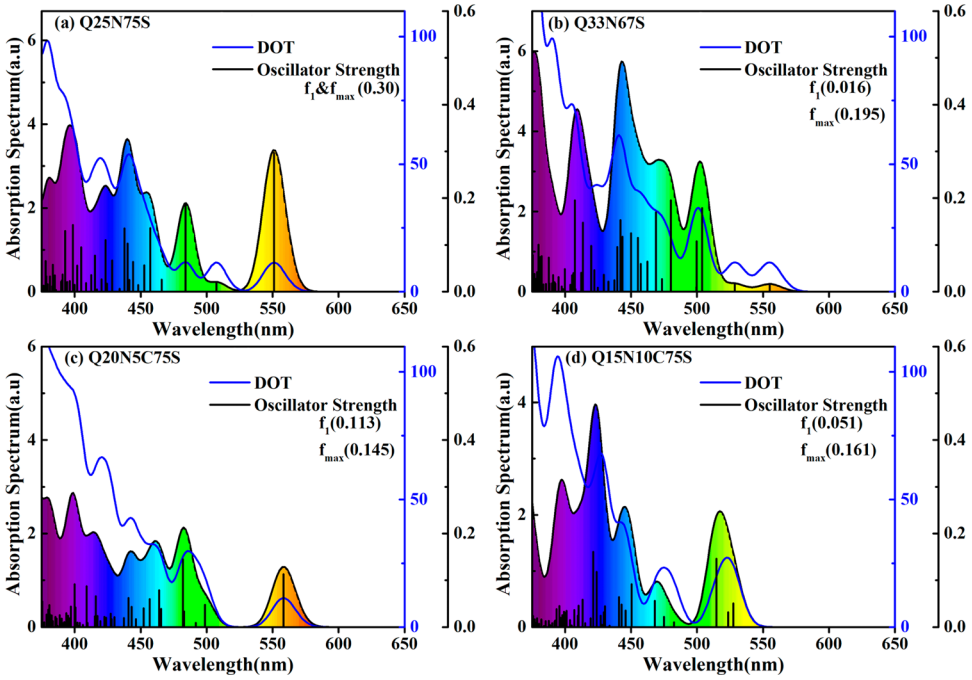

Figure 3. Absorption spectra of $Cd_{33}Se_{33}$ QDs embedded in glass matrices. The calculated structure is the final configuration of the 10 ps AIMD production run (Figure 2). The first absorption peak is redshifted compared to that of the pristine QD, and the oscillator strength of the lowest-energy transition varies depending on the composition of glass matrices.

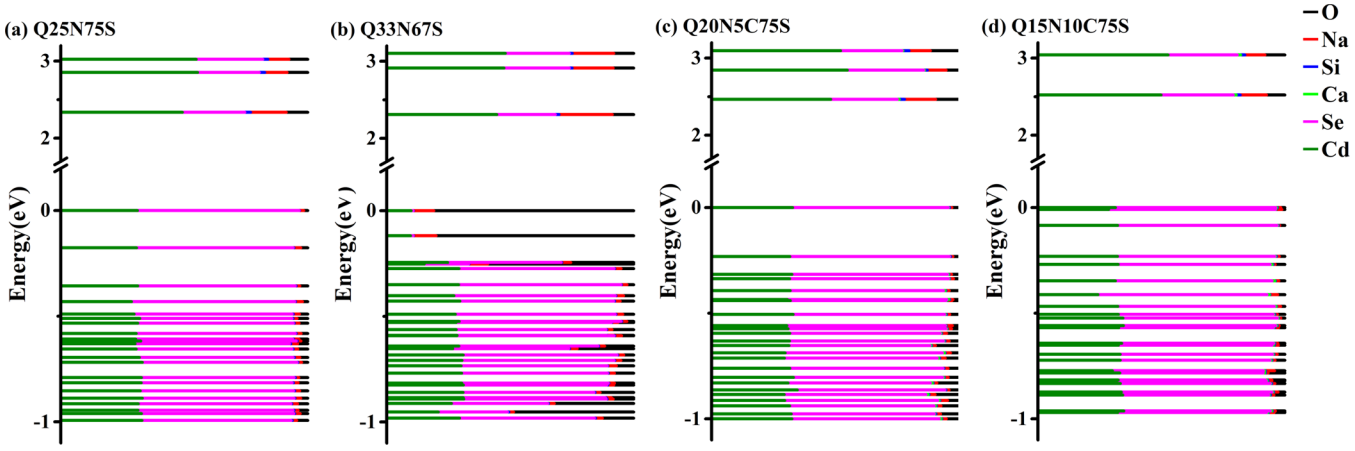

Figure 4. Computed electronic structure of the CdSe QDs embedded in glasses. The calculated structure is the final configuration of the 10 ps AIMD production run. Each line corresponding to a molecular orbital and HOMO was set at 0 eV. Each color represents the contribution of a type of atom for a given molecular orbital. Apparently, the HOMO of Q33N67S is mainly determined by O atoms rather than Se atoms in other compositions.

interacting electron and hole pair for CdS QDs in phosphate glass was experimentally observed by optically detected magnetic resonance (ODMR) spectroscopy, suggesting a localized state at the surface of CdS QDs.[54] The origin of this interfacially localized state could not be clarified by the ODMR; however, nonbridging oxygen atoms might be the source according to our study. For this composition, the HOMO-2 orbital is still localized on the interfacial nonbridging oxygen atoms (Figure S5a). It changes to a simultaneous distribution on the hybrid QD and interfacial nonbridging oxygen atoms (Figure S5b) for the HOMO-3 orbital, which corresponds to the third excited-state transition with an oscillator strength equal to 0.18. The brightest peak with the maximum oscillator transition is located at 2.58 eV (sixth excited-state transition), principally originating from the transition from HOMO-5 (Figure S5d) to LUMO. The HOMO-5 orbital is mostly distributed on the hybrid QD. It is clear that the charge density distribution shifts from the glass matrices to the hybrid QD gradually with the decrease of energy of occupied orbitals. Before the brightest peak, there are a number of low-energy states with weak oscillator strength, demonstrating the possibility of an absorption tail.

Based on our previous study,[39] the HOMO of most of the configurations was decided by nonbridging oxygen, while it was determined by Se atoms in 7 out of 50 configurations of Q33N67S glasses. To check this, we selected another four configurations to conduct further TDDFT calculations (presented in Figures S6 and S7). In most configurations, a weakly absorptive tail due to a dense manifold of low-lying states before the brightest peak can be observed, regardless of whether the HOMO is localized on interfacial nonbridging oxygen or uncoordinated surface Se atoms (Figure S7a,b). Although the

https://doi.org/10.1021/jacs.2c03039
J. Am. Chem. Soc. 2022, 144, 11296−11305

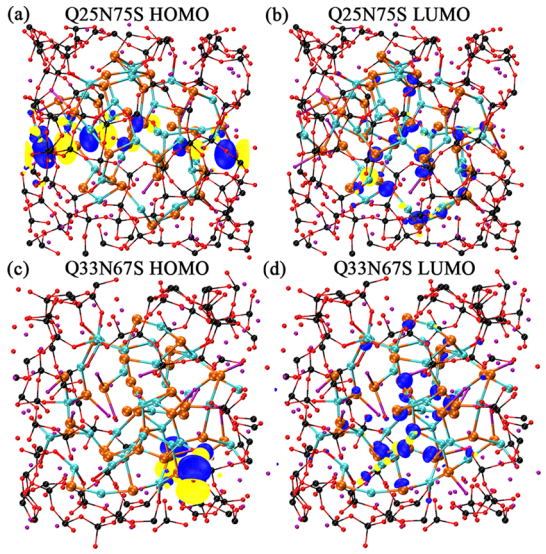

Figure 5. Molecular orbitals of CdSe QDs embedded in inorganic glass matrices. The distribution of charge density of Q25N75S and Q33N67S glasses. The HOMO is localized on the nonbridging oxygens at the QD/glass interface in Q33N67S glasses, while the LUMO is delocalized on the CdSe QDs, indicating the weak oscillator strength of the lowest-energy transition due to the small overlap of hole and electron wave functions. A drawing of partial enlargement is provided in Figure S3.

oscillator strength of the lowest-energy transition is bigger in some configurations of Q33N67S glasses, it is still lower than that of Q25N75S glasses.

Moreover, the oscillator strength of the first excited-state transition of Q20N5C75S and Q15N10C75S glasses is also higher than that of Q33N67S glasses. Based on the analysis of charge density distribution of molecular orbitals contributing to the lowest-energy transition (Figures 6 and S8), the hybridized nature of these orbitals is clear with most of them distributed on the surface Se atoms and a small portion on nonbridging oxygen atoms. The localization of HOMO for Q20N5C75S and Q15N10C75S glasses is not as significant as Q33N67S glasses, resulting in a bigger overlap of electron and hole wave functions.

It is well known that the timescale of electron relaxation to the band edge states is in a picosecond range, while the emission is in a nanosecond range. As such, it is reasonable to assume that emission takes place from the lowest-energy states if it is optically active (large oscillator strength) since it is much faster than the nonradiative recombination via interband multiple phonon processes. However, if the lowest-energy states are optically weak (small oscillator strength) or even completely inactive, it takes much longer for radiative emission; in this case, nonradiative processes can take place and even quench the emission. Therefore, the oscillator strength of the lowest-energy transition (which is inversely proportional to the radiative time) could be used as an indicator of the emission efficiency of the QDs.[27,31] In terms of experimental characterization, the PLQY is a common index to represent emission efficiency. Therefore, based on our calculations, the PLQY of the glasses is expected to decrease in the order of Q25N75S, Q20N5C75S, Q15N5C75S, and Q33N67S according to the oscillator strength of the first excited-state transition.

To test the validity of our model, glasses with nominal compositions (mol %) of 25 Na_2O−75 SiO_2−1 CdSe, 33 Na_2O−67 SiO_2−1 CdSe, 20 Na_2O−5 CaO−75 SiO_2−1 CdSe, and 15 Na_2O−10 CaO−75 SiO_2−1 CdSe were experimentally fabricated (see Supporting Information for details about fabrication and characterization methods). For all glass samples, the first excitonic absorption peak is located at 444 nm (Figure 7a). Moreover, the absorption tails are obvious in Q33N67S, Q20N5C75S, and Q15N10C75S glasses. In Figure 3, a number of low-energy states with weak oscillator strength below the brightest peak are observed in glasses except for Q25N75S glasses, indicating that the absorption tail originates from those states, consistent with the experimental findings.

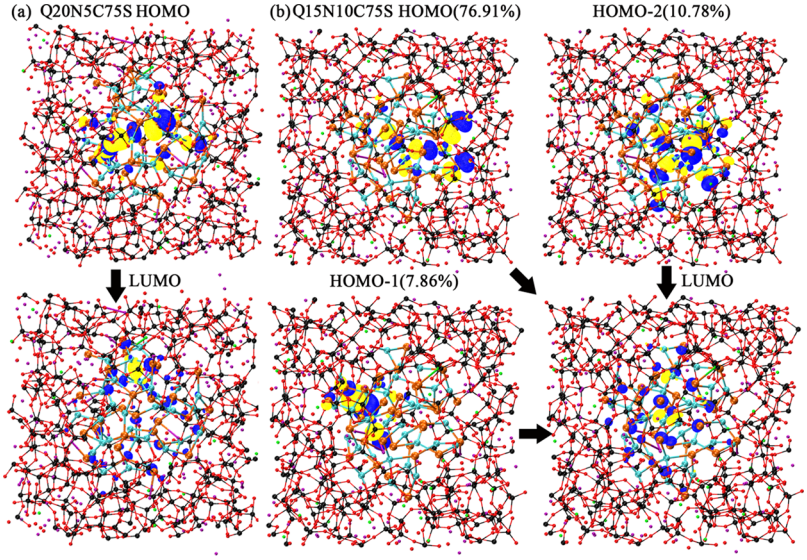

Figure 6. Molecular orbitals of CdSe QDs embedded in inorganic glass matrices. (a) Charge density distribution of the HOMO (top left) and LUMO (bottom left) of Q20N5C75S glasses. (b) Charge density distribution of the HOMO, HOMO-1, HOMO-2, and LUMO of Q15N10C75S glasses. The percentage represents the contribution of the transition from each orbital to LUMO of the lowest-energy transition. All contributions higher than 5% are listed. All the charge densities of frontier orbitals are mainly distributed on Se atoms with a small portion on interfacial nonbridging oxygens, reflecting the hybridized nature of these frontier orbitals. A drawing of partial enlargement is provided in Figure S8.

https://doi.org/10.1021/jacs.2c03039
J. Am. Chem. Soc. 2022, 144, 11296−11305

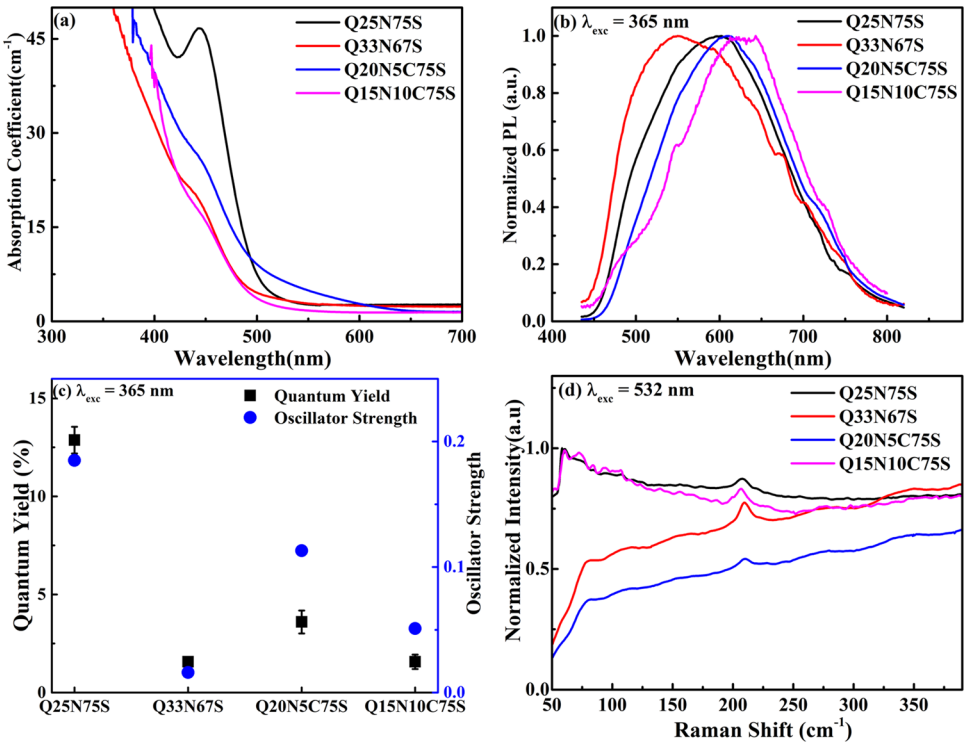

Figure 7. (a) Absorption spectra, (b) normalized PL spectra (recorded under 365 nm excitation), (c) quantum yield (left *y*-axis) and oscillator strength (right *y*-axis) of the lowest-energy states in our model, and (d) Raman spectra (recorded under 532 nm excitation) of Q25N75S, Q33N67S, Q20N5C75S, and Q15N10C75S glasses heat-treated at 530 °C for 20 h, 480 °C for 20 h, 560 °C for 10 h, and 580 °C for 40 h, respectively. The error bar reflects the standard deviation of the measurement of PLQY. The PLQYs of the experimental fabricated glass samples are consistent with the oscillator strength as the computational simulation predicted.

A Raman peak at 205 cm^{-1} was observed for all samples, in good agreement with the longitudinal optical phonon of CdSe (Figure 7d).[55] Based on the first excitonic absorption peak using the empirical equation,[56] the calculated size of the CdSe QDs formed in the glass specimen is 1.9 nm, which is bigger than that of pristine $Cd_{33}Se_{33}$ (1.3 nm) and hybrid $Cd_{33}Se_{33}$ (~1.6 nm) in our computational model. It is hard to synthesize CdSe QDs with a small size in glass matrices and this size was the smallest one we could achieve experimentally: our models based on $Cd_{33}Se_{33}$ already contain around 1100 atoms in total (including the glass), which is at the limit of computationally accessible systems. Thus, one might question the relevance of our results to realistic CdSe QDs formed in glasses. Goldzak et al.[36] tested the size dependence of the excited states of $Cd_{33}Se_{33}$ (1.3 nm), $Cd_{38}Se_{38}$ (1.4 nm), and $Cd_{91}Se_{91}$ (2 nm). These authors found that the number of low-energy states below the brightest state was likely to be larger with the increase in the radius of CdSe QDs. This observation suggests that the localization of the hole on undercoordinated Se atoms seems to be more obvious for CdSe within the experimental range.

Although the positions of the absorption peak of these glass samples are the same, the emission peaks are located in different ranges under 365 nm light excitation (Figure 7b), indicating the various low-energy surface states of CdSe QDs in glass matrices. In addition, the PLQY is 12.87, 1.57, 3.6, and 1.57% for Q25N75S, Q33N67S, Q20N5C75S, and Q15N10C75S glasses, respectively (Figure 7c). As the oscillator strength of the lowest-energy transition can be an indicator of emissive properties, the tendency of the PLQYs in experiments is the same as the oscillator strengths in our computational simulation, validating the accuracy of our model.

The large Stokes shift, the broad full width at half maximum (FWHM) of emission peaks, and the low PLQYs demonstrate the disappearance of intrinsic emission from the pristine QD. These observations can be explained by our model. First of all, the dense manifold of low-energy states below the brightest peak provides intermediate states for the relaxing of electrons, explaining the observed bigger Stokes shift. Second, the micro region of CdSe QDs embedded in glasses is inhomogeneous due to the fluctuation of temperature and composition during realistic fabrication, leading to various interactions between the CdSe QDs and glass matrices. The luminescence of the CdSe QDs embedded in glasses originates from the combination of emission from these micro regions. According to our simulation, the excited states of the hybrid QD in different glass matrices are diverse. For example, based on the oscillator strength and excitation energy of the lowest-energy transition of the configuration shown in Figures S4 and S6, the combination of emission from these configurations can be obtained, exhibiting similar broad emission as the experimental findings (Figure S9). Therefore, the observed broad emission and large FWHM are derived from the various structures of the hybrid QD.

Finally, the unavoidable structural construction contributed to the formation of undercoordinated Se atoms or Cd atoms at the QD/glass interface and breakage of Cd−Se bonds even in the core, resulting in the disappearance of the pristine QD. At the same time, the presence of CdSe QDs also leads to the inevitable formation of nonbridging oxygen atoms at the interface. The undercoordinated Se atoms and nonbridging oxygen atoms give rise to the localization of the hole wave function, further decreasing the overlap between the electron and hole wave functions and forming low-energy states with

https://doi.org/10.1021/jacs.2c03039
J. Am. Chem. Soc. 2022, 144, 11296−11305

weak oscillator strength. These low-lying states with very long emission lifetimes give a larger window for nonradiative processes to decrease the PLQY. The disappearance of the pristine QD and the inherent undercoordinated Se atoms or nonbridging oxygen atoms at the QD/glass interface are the origin of low PLQYs of CdSe QDs embedded in glass matrices.

One may question that why the PLQY of Q25N75S glasses is smaller though the oscillator strength is much higher than that of the pristine QD. This may be attributed to the limitation of our model. For one thing, the size of CdSe QDs (~1.9 nm) in the experiment is much bigger than that of the pristine CdSe QD (~1.3 nm), and the number of low-energy states with small oscillator strength increases with the QD radius,[36] suggesting that the localized interfacial states are more severe in the experiment range. We also note that our atomistic model is a simplified model with a perfect CdSe QD initially incorporated into the glass matrices. However, the real atomic structure is far more complicated such as vacancy and nonstoichiometric QD not being considered in our model. These defects may also decrease the PLQYs of CdSe QDs embedded in glasses.

3. CONCLUSIONS AND PERSPECTIVES

In conclusion, our theoretical results pinpoint the origin of the low PLQY of CdSe QDs embedded in inorganic matrices. By simulating the $Cd_{33}Se_{33}$ QD embedded in various glasses, we observed the formation of undercoordinated Se atoms and nonbridging oxygen atoms at the QD/glass interface, leading to the localization of the hole wave function. The overlap between these localized states and delocalized electron states is small, resulting in a dense manifold of low-energy lying states with weak oscillator strength, further providing large opportunities for nonradiative processes hindering radiative emission. The glass matrices therefore have a significant impact on the emissive properties of CdSe QDs embedded in glasses, which is indicated by the different excitation energies and oscillator strengths of the lowest-energy excited states. The experimentally measured PLQYs of the QD/glass system are in good agreement with our theoretical simulations, demonstrating the validity of our model.

Our results may provide guidance for both experimentalists and theorists to address the long-troubled low PLQY problem, paving the way for practical application of QDs embedded in inorganic matrices ranging from LED to next-generation displays. We suggest that the composition of glass matrices, and especially the presence of the nonbridging oxygen atoms, is crucial to the luminescence properties. Glass matrices with a low ratio of glass modifiers are found to exhibit better optical performance, which is one direction to adjust the glass composition. Additionally, although it is tough to passivate QDs in glasses, the passivation method focused on nonbridging oxygen atoms and Se atoms is supposed to be effective. It also can be applied to passivate colloidal QDs with an inorganic shell such as SiO_2. As a common method to calculate the radius of CdSe QDs in glasses based on the absorption peak, our results also suggest that the band gap can be different for QDs with the same size in different glass matrices. Therefore, this suggested caution in using these empirical equations.

Finally, our present computational study focused on stoichiometric QDs, while nonstoichiometric QDs are more common in reality. The Se-rich CdSe QD was found to have poor PL performance compared to the Cd-rich CdSe QD and stoichiometric QDs.[31] It is worth considering this imperfect QD embedded in glasses, and the semiconductor material is not limited to CdSe, PbS, or perovskite QD. Another obvious extension would involve exploring faster computational methodologies to investigate the excited states of QDs with larger sizes, directly within the experimental range. The combining of machine learning with DFT calculation may be one solution to solve this problem.

4. METHODS

4.1. Creating the Atomic Structure of CdSe QDs Embedded in Inorganic Matrices. The generation of CdSe QDs embedded in glass matrices involves three steps as developed in our previous study.[38] First, the glass matrices with a composition of 25 Na_2O−75 SiO_2, 33 Na_2O−67 SiO_2, 20 Na_2O−5 CaO−75 SiO_2, and 15 Na_2O−10 CaO−75 SiO_2 (mol %) were generated by classical MD simulations using the DL_POLY code.[57] A partial-charge rigid-ion pairwise potential developed by Pedone et al.[58] was used to perform the simulations. The Coulomb interactions were calculated using the Ewald summation method[59] with a precision of 10^{-5}, and the real-space cutoff for short-range interactions was set to 7.6 Å. The initial configurations were obtained by randomly placing the atoms in a cubic simulation cell, with the density consistent with the experimental values. The final configurations were generated by a melt-quenching approach in an *NVT* ensemble. The initial structure was heated up gradually in steps of 1000 K with a 60 ps MD run at each temperature from 300 to 6000 K. After equilibration of the liquid at 6000 K during 400 ps, the system was cooled gradually in steps of 500 K with a 60 ps MD run at each temperature from 6000 to 300 K. A further 200 ps *NVT* simulation was carried out at 300 K together with a 200 ps *NVE* simulation in order to equilibrate the structure.

Second, a perfect $Cd_{33}Se_{33}$ QD was incorporated into the obtained glass matrices, which served as the initial configuration for classical MD simulations. Some atoms were removed from the glass matrices to keep the interatomic distance between the CdSe QD and glass matrices longer than 2.5 Å. The number of the atoms of the resulting structure (Table S1) was 30 Na_2O−90 SiO_2−33 CdSe, 39 Na_2O−78 SiO_2−33 CdSe, 68 Na_2O−17 CaO−255 SiO_2−33 CdSe, and 51 Na_2O−34 CaO−255 SiO_2−33 CdSe, as shown in Figure S1. The interatomic interactions in CdSe QDs were described by a Lenard-Jones pairwise potential validated in CdSe nanocrystals,[60,61] and the Lorentz−Berthelot combining rules were used for the interactions between the CdSe QD and glass matrices. The whole structure was first equilibrated at 1000 K using 200 ps of *NVT* dynamics followed by 200 ps of *NVE* dynamics. Then, it was cooled gradually from 1000 to 500 K while keeping CdSe frozen to keep the integrity of the CdSe QD. Subsequent cooling from 500 to 300 K took place in steps of 10 K with all atoms allowed to move. Finally, the structures were equilibrated at 300 K with 200 ps of *NVT* and *NVE* dynamics.

Third, the final configuration of the classical MD simulation was used as the initial configuration for AIMD using the CP2K code.[62] The PBE exchange-correlation functional at the generalized gradient approximation level was employed.[63] For Na, Ca, Cd, and Se, a short-range molecularly optimized double-ζ single polarized basis set (DZVP-MOLOPT-SR-GTH) was used, while for O and Si, we used a double-ζ single polarized basis set (DZVP-MOLOPT-GTH).[64,65] The plane wave cutoff and relative cutoff were set to 600 Ry and 40 Ry, respectively. The structure was quenched from 500 to 300 K in steps of 50 K with a total 10 ps AIMD run at each temperature with a time step of 2 fs. The production run was conducted in the *NVT* ensemble at 300 K for 10 ps.

4.2. Electronic Structure Calculation of CdSe QDs Embedded in Inorganic Matrices. The final configuration of the AIMD run (Figure 2) was used to conduct a ground-state electronic structure calculation. The PBE0-TC-LRC exchange-correlation functional[66] with a cutoff radius of 4 Å was employed to calculate the molecular orbitals of those configurations with the auxiliary density matrix method.[67] The same basis set and cutoff were employed in the electronic structure calculations as the AIMD run. The absorption spectra were calculated using linear response TDDFT as implemented in the CP2K code, with the same functional and basis set as used in the ground-state

https://doi.org/10.1021/jacs.2c03039
J. Am. Chem. Soc. 2022, 144, 11296−11305

calculations. The excitations of the first 100 electronic transition states were calculated. The obtained oscillator strength and excitation energy were broadened by the Gaussian function with a line width of 35 meV to obtain the absorption spectra. The excitation energies were also broadened with the same linewidth to calculate the density of transitions.

■ ASSOCIATED CONTENT

Supporting Information

The Supporting Information is available free of charge at https://pubs.acs.org/doi/10.1021/jacs.2c03039.

Absorption spectra and plots of frontier molecular orbitals of some representative configurations together with the details of experimental and characterization method (PDF)

TDDFT input files and geometry structure in the .xyz format used for TDDFT calculations (ZIP)

■ AUTHOR INFORMATION

Corresponding Authors

Chao Liu − *State Key Laboratory of Silicate Materials for Architectures, Wuhan University of Technology, Hubei 430070, China;* orcid.org/0000-0003-4324-6409; Email: hite@whut.edu.cn

François-Xavier Coudert − *Chimie ParisTech, PSL University, CNRS, Institut de Recherche de Chimie Paris, Paris 75005, France;* orcid.org/0000-0001-5318-3910; Email: fx.coudert@chimieparistech.psl.eu

Authors

Wenke Li − *State Key Laboratory of Silicate Materials for Architectures, Wuhan University of Technology, Hubei 430070, China; Chimie ParisTech, PSL University, CNRS, Institut de Recherche de Chimie Paris, Paris 75005, France;* orcid.org/0000-0001-9018-7769

Kai Li − *State Key Laboratory of Silicate Materials for Architectures, Wuhan University of Technology, Hubei 430070, China*

Xiujian Zhao − *State Key Laboratory of Silicate Materials for Architectures, Wuhan University of Technology, Hubei 430070, China;* orcid.org/0000-0002-2517-2605

Complete contact information is available at: https://pubs.acs.org/10.1021/jacs.2c03039

Notes

The authors declare no competing financial interest.

The representative input files for the calculations are available online at https://github.com/fxcoudert/citable-data.

■ ACKNOWLEDGMENTS

This work was financially supported by the National Natural Science Foundation of China (grant no. 62175192). We acknowledge access to high-performance computing platforms provided by GENCI grant A0110807069.

■ REFERENCES

(1) Ekimov, A. I.; Onushchenko, A. A. Quantum Size Effect in Three-Dimensional Microscopic Semiconductor Crystals. *JETP Lett.* **1981**, *34*, 345−348.

(2) Rossetti, R.; Ellison, J. L.; Gibson, J. M.; Brus, L. E. Size Effects in the Excited Electronic States of Small Colloidal CdS crystallites. *J. Chem. Phys.* **1984**, *80*, 4464−4469.

(3) Yang, Y.; Zheng, Y.; Cao, W.; Titov, A.; Hyvonen, J.; Manders, J. R.; Xue, J.; Holloway, P. H.; Qian, L. High-efficiency Light-Emitting Devices Based on Quantum Dots with Tailored Nanostructures. *Nat. Photonics* **2015**, *9*, 259−266.

(4) Gualdrón-Reyes, A. F.; Meléndez, A. M.; Tirado, J.; Mejia-Escobar, M. A.; Jaramillo, F.; Niño-Gómez, M. E. Hidden Energy Levels? Carrier Transport Ability of $CdS/CdS_{1-x}Se_x$ Quantum Dot Solar Cells Impacted by Cd-Cd Level Formation. *Nanoscale* **2019**, *11*, 762−774.

(5) Fan, F.; Voznyy, O.; Sabatini, R. P.; Bicanic, K. T.; Adachi, M. M.; McBride, J. R.; Reid, K. R.; Park, Y. S.; Li, X.; Jain, A.; Quintero-Bermudez, R.; Saravanapavanantham, M.; Liu, M.; Korkusinski, M.; Hawrylak, P.; Klimov, V. I.; Rosenthal, S. J.; Hoogland, S.; Sargent, E. H. Continuous-wave Lasing in Colloidal Quantum Dot Solids Enabled by Facet-Selective Epitaxy. *Nature* **2017**, *544*, 75−79.

(6) Heuer-Jungemann, A.; Feliu, N.; Bakaimi, I.; Hamaly, M.; Alkilany, A.; Chakraborty, I.; Masood, A.; Casula, M. F.; Kostopoulou, A.; Oh, E.; Susumu, K.; Stewart, M. H.; Medintz, I. L.; Stratakis, E.; Parak, W. J.; Kanaras, A. G. The Role of Ligands in the Chemical Synthesis and Applications of Inorganic Nanoparticles. *Chem. Rev.* **2019**, *119*, 4819−4880.

(7) Xu, L.; Liang, H. W.; Yang, Y.; Yu, S. H. Stability and Reactivity: Positive and Negative Aspects for Nanoparticle Processing. *Chem. Rev.* **2018**, *118*, 3209−3250.

(8) Jing, L.; Kershaw, S. V.; Li, Y.; Huang, X.; Li, Y.; Rogach, A. L.; Gao, M. Aqueous Based Semiconductor Nanocrystals. *Chem. Rev.* **2016**, *116*, 10623−10730.

(9) Nasilowski, M.; Spinicelli, P.; Patriarche, G.; Dubertret, B. Gradient CdSe/CdS Quantum Dots with Room Temperature Biexciton Unity Quantum Yield. *Nano Lett.* **2015**, *15*, 3953−3958.

(10) Liu, F.; Zhang, Y.; Ding, C.; Kobayashi, S.; Izuishi, T.; Nakazawa, N.; Toyoda, T.; Ohta, T.; Hayase, S.; Minemoto, T.; Yoshino, K.; Dai, S.; Shen, Q. Highly Luminescent Phase-Stable $CsPbI_3$ Perovskite Quantum Dots Achieving Near 100% Absolute Photoluminescence Quantum Yield. *ACS Nano* **2017**, *11*, 10373−10383.

(11) Xia, M.; Liu, C.; Zhao, Z.; Wang, J.; Lin, C.; Xu, Y.; Heo, J.; Dai, S.; Han, J.; Zhao, X. Surface Passivation of CdSe Quantum Dots in All Inorganic Amorphous Solid by Forming $Cd_{1-x}Zn_xSe$ Shell. *Sci. Rep.* **2017**, *7*, 42359.

(12) Han, K.; Im, W. B.; Heo, J.; Chung, W. J. A Complete Inorganic Colour Converter Based on Quantum-Dot-Embedded Silicate Glasses for White Light-Emitting-Diodes. *Chem. Commun.* **2016**, *52*, 3564−3567.

(13) Bell, G.; Filin, A. I.; Romanov, D. A.; Levis, R. J. Direct growth of CdSe Semiconductor Quantum Dots in Glass Matrices by femtosecond Laser Beam. *Appl. Phys. Lett.* **2016**, *108*, No. 063112.

(14) Han, K.; Yoon, S.; Chung, W. J. CdS and CdSe Quantum Dot-Embedded Silicate Glasses for LED Color Converter. *Int. J. Appl. Glass Sci.* **2015**, *6*, 103−108.

(15) Liu, C.; Heo, J.; Zhang, X.; Adam, J.-L. Photoluminescence of PbS Quantum Dots Embedded in Glasses. *J. Non-Cryst. Solids* **2008**, *354*, 618−623.

(16) Xia, M.; Zhu, S.; Luo, J.; Xu, Y.; Tian, P.; Niu, G.; Tang, J. Ultrastable Perovskite Nanocrystals in All-Inorganic Transparent Matrices for High-Speed Underwater Wireless Optical Communication. *Adv. Opt. Mater.* **2021**, *9*, No. 2002239.

(17) Ye, Y.; Zhang, W.; Zhao, Z.; Wang, J.; Liu, C.; Deng, Z.; Zhao, X.; Han, J. Highly Luminescent Cesium Lead Halide Perovskite Nanocrystals Stabilized in Glasses for Light-Emitting Applications. *Adv. Opt. Mater.* **2019**, *7*, No. 1801633.

(18) Zhang, X.; Guo, L.; Zhang, Y.; Cheng, C.; Cheng, Y.; Li, X.; Zhang, J.; Xu, S.; Cao, Y.; Sun, J.; Cheng, L.; Chen, B. Improved Photoluminescence Quantum Yield of $CsPbBr_3$ Quantum Dots Glass Ceramics. *J. Am. Ceram. Soc.* **2020**, *103*, 5028−5035.

(19) Kıbrıslı, O.; Erol, E.; Çelikbilek Ersundu, M.; Ersundu, A. E. Robust $CsPbBr_3$ and $CdSe/Dy^{3+}$+CdSe Quantum Dot Doped Glass Nanocomposite Hybrid Coupling as Color Converter for Solid-State Lighting Applications. *Chem. Eng. J.* **2021**, *420*, No. 130542.

(20) Lin, M.; Zhang, X.; Guo, L.; Zhang, Y.; Song, R.; Xu, S.; Zhu, H.; Cheng, C.; Cao, Y.; Wang, Y.; Chen, B. Blue and Green Light Exciton Emission of Chloro-Brominated Perovskite Quantum Dots Glasses. *Opt. Mater.* **2021**, *122*, No. 111654.
(21) Lipatova, Z. O.; Kolobkova, E. V.; Babkina, A. N. Luminescent Properties of Cadmium Selenide Quantum Dots in Fluorophosphate Glasses. *Opt. Spectrosc.* **2016**, *121*, 713−721.
(22) Yu, M.; Fernando, G. W.; Li, R.; Papadimitrakopoulos, F.; Shi, N.; Ramprasad, R. First Principles Study of CdSe Quantum Dots: Stability, Surface Unsaturations, and Experimental Validation. *Appl. Phys. Lett.* **2006**, *88*, 231910.
(23) Houtepen, A. J.; Hens, Z.; Owen, J. S.; Infante, I. On the Origin of Surface Traps in Colloidal II−VI Semiconductor Nanocrystals. *Chem. Mater.* **2017**, *29*, 752−761.
(24) Puzder, A.; Williamson, A. J.; Zaitseva, N.; Galli, G.; Manna, L.; Alivisatos, A. P. The Effect of Organic Ligand Binding on the Growth of CdSe Nanoparticles Probed by Ab Initio Calculations. *Nano Lett.* **2004**, *4*, 2361−2365.
(25) Puzder, A.; Williamson, A. J.; Gygi, F.; Galli, G. Self-Healing of CdSe Nanocrystals: First-Principles Calculations. *Phys. Rev. Lett.* **2004**, *92*, No. 217401.
(26) Kilina, S. V.; Tamukong, P. K.; Kilin, D. S. Surface Chemistry of Semiconducting Quantum Dots: Theoretical Perspectives. *Acc. Chem. Res.* **2016**, *49*, 2127−2135.
(27) Lystrom, L.; Roberts, A.; Dandu, N.; Kilina, S. Surface-Induced Deprotonation of Thiol Ligands Impacts the Optical Response of CdS Quantum Dots. *Chem. Mater.* **2021**, *33*, 892−901.
(28) Nguyen, K. A.; Pachter, R.; Day, P. N. Computational Prediction of Structures and Optical Excitations for Nanoscale Ultrasmall ZnS and CdSe Clusters. *J. Chem. Theory Comput.* **2013**, *9*, 3581−3596.
(29) Kilina, S.; Cui, P.; Fischer, S. A.; Tretiak, S. Conditions for Directional Charge Transfer in CdSe Quantum Dots Functionalized by Ru(II) Polypyridine Complexes. *J. Phys. Chem. Lett.* **2014**, *5*, 3565−3576.
(30) Troparevsky, M. C.; Kronik, L.; Chelikowsky, J. R. Optical Properties of CdSe Quantum Dots. *J. Chem. Phys.* **2003**, *119*, 2284−2287.
(31) Bhati, M.; Ivanov, S. A.; Senftle, T. P.; Tretiak, S.; Ghosh, D. Nature of Electronic Excitations in Small Non-Stoichiometric Quantum Dots. *J. Mater. Chem. A* **2022**, *10*, 5212−5220.
(32) Jose, R.; Zhanpeisov, N. U.; Fukumura, H.; Baba, Y.; Ishikawa, M. Structure-Property Correlation of CdSe Clusters Using Experimental Results and First-Principles DFT Calculations. *J. Am. Chem. Soc.* **2006**, *128*, 629−636.
(33) Kilina, S.; Ivanov, S.; Tretiak, S. Effect of Surface Ligands on Optical and Electronic Spectra of Semiconductor Nanoclusters. *J. Am. Chem. Soc.* **2009**, *131*, 7717−7726.
(34) Trivedi, D. J.; Wang, L.; Prezhdo, O. V. Auger-Mediated Electron Relaxation is Robust to Deep Hole Traps: Time-Domain Ab Initio Study of CdSe Quantum Dots. *Nano Lett.* **2015**, *15*, 2086−2091.
(35) Fischer, S. A.; Crotty, A. M.; Kilina, S. V.; Ivanov, S. A.; Tretiak, S. Passivating Ligand and Solvent Contributions to the Electronic Properties of Semiconductor Nanocrystals. *Nanoscale* **2012**, *4*, 904−914.
(36) Goldzak, T.; McIsaac, A. R.; Van Voorhis, T. Colloidal CdSe Nanocrystals are Inherently Defective. *Nat. Commun.* **2021**, *12*, 890.
(37) Baskoutas, S.; Terzis, A. F. Size-Dependent Band Gap of Colloidal Quantum Dots. *J. Appl. Phys.* **2006**, *99*, No. 013708.
(38) Li, W.; Zhao, X.; Liu, C.; Coudert, F. X. Ab Initio Molecular Dynamics of CdSe Quantum-Dot-Doped Glasses. *J. Am. Chem. Soc.* **2020**, *142*, 3905−3912.
(39) Li, W.; Zhao, X.; Liu, C.; Coudert, F.-X. Influence of Glass Composition on the Luminescence Mechanisms of CdSe Quantum-Dot-Doped Glasses. *J. Phys. Chem. C* **2021**, *125*, 18916−18926.
(40) Li, W.; Li, N.; Liu, C.; Greaves, G. N.; Ong, W. J.; Zhao, X. Understanding the Atomic and Electronic Structures Origin of Defect Luminescence of CdSe Quantum Dots in Glass Matrices. *J. Am. Ceram. Soc.* **2019**, *102*, 5375−5385.
(41) Albert, V. V.; Ivanov, S. A.; Tretiak, S.; Kilina, S. V. Electronic Structure of Ligated CdSe Clusters: Dependence on DFT Methodology. *J. Phys. Chem. C* **2011**, *115*, 15793−15800.
(42) Kasuya, A.; Sivamohan, R.; Barnakov, Y. A.; Dmitruk, I. M.; Nirasawa, T.; Romanyuk, V. R.; Kumar, V.; Mamykin, S. V.; Tohji, K.; Jeyadevan, B.; Shinoda, K.; Kudo, T.; Terasaki, O.; Liu, Z.; Belosludov, R. V.; Sundararajan, V.; Kawazoe, Y. Ultra-Stable Nanoparticles of CdSe Revealed from Mass Spectrometry. *Nat. Mater.* **2004**, *3*, 99−102.
(43) Tamukong, P. K.; Peiris, W. D.; Kilina, S. Computational Insights into CdSe Quantum Dots' Interactions with Acetate Ligands. *Phys. Chem. Chem. Phys.* **2016**, *18*, 20499−20510.
(44) Ellis, J. L.; Hickstein, D. D.; Schnitzenbaumer, K. J.; Wilker, M. B.; Palm, B. B.; Jimenez, J. L.; Dukovic, G.; Kapteyn, H. C.; Murnane, M. M.; Xiong, W. Solvents Effects on Charge Transfer from Quantum Dots. *J. Am. Chem. Soc.* **2015**, *137*, 3759−3762.
(45) Lo, S. S.; Khan, Y.; Jones, M.; Scholes, G. D. Temperature and Solvent Dependence of CdSe/CdTe Heterostructure Nanorod Spectra. *J. Chem. Phys.* **2009**, *131*, No. 084714.
(46) Wuister, S. F.; de Mello Donega, C.; Meijerink, A. Local-field Effects on the Spontaneous Emission Rate of CdTe and CdSe Quantum Dots in Dielectric Media. *J. Chem. Phys.* **2004**, *121*, 4310−4315.
(47) Ibnaouf, K. H.; Prasad, S.; Al Salhi, M. S.; Hamdan, A.; Zaman, M. B.; El Mir, L. Influence of the Solvent Environments on the Spectral Features of CdSe Quantum Dots with and without ZnS Shell. *J. Lumin.* **2014**, *149*, 369−373.
(48) Nguyen, K. A.; Day, P. N.; Pachter, R. Understanding Structural and Optical Properties of Nanoscale CdSe Magic-Size Quantum Dots: Insight from Computational Prediction. *J. Phys. Chem. C* **2010**, *114*, 16197−16209.
(49) Oh, M. H. J.; Chen, M.; Chuang, C.-H.; Wilson, G. J.; Burda, C.; Winnik, M. A.; Scholes, G. D. Charge Transfer in CdSe Nanocrystal Complexes with an Electroactive Polymer. *J. Phys. Chem. C* **2013**, *117*, 18870−18884.
(50) Takagahara, T. Effects of Dielectric Confinement and Electron-Hole Exchange Interaction on Excitonic States in Semiconductor Quantum Dots. *Phys. Rev. B* **1993**, *47*, 4569−4584.
(51) Wang, Y.; Herron, N. Nanometer-Sized Semiconductor Clusters: Materials Synthesis, Quantum Size Effects, and Photophysical Properties. *J. Phys. Chem.* **1991**, *95*, 525−532.
(52) Hsieh, C. H.; Jain, H.; Kamitsos, E. I. Correlation between Dielectric Constant and Chemical Structure of Sodium Silicate Glasses. *J. Appl. Phys.* **1996**, *80*, 1704−1712.
(53) Wang, L.-W.; Zunger, A. Pseudopotential Calculations of Nanoscale CdSe Quantum Dots. *Phys. Rev. B* **1996**, *53*, 9579−9582.
(54) Lifshitz, E.; Glozman, A.; Litvin, I. D.; Porteanu, H. Optically Detected Magnetic Resonance Studies of the Surface-Interface Properties of II-VI Semiconductor Quantum Dots. *J. Phys. Chem. B* **2000**, *104*, 10449−10461.
(55) Hwang, Y.-N.; Shin, S.; Park, H. L.; Park, S.-H.; Kim, U.; Jeong, H. S.; Shin, E. J.; Kim, D. Effect of Lattice Contraction on the Raman Shifts of CdSe Quantum Dots in Glass Matrices. *Phys. Rev. B* **1996**, *54*, 15120−15124.
(56) Yu, W. W.; Qu, L.; Guo, W.; Peng, X. Experimental Determination of the Extinction Coefficient of CdTe, CdSe, and CdS Nanocrystals. *Chem. Mater.* **2003**, *15*, 2854−2860.
(57) Smith, W.; Yong, C. W.; Rodger, P. M. DL_POLY: Application to Molecular Simulation. *Mol. Simul.* **2010**, *28*, 385−471.
(58) Pedone, A.; Malavasi, G.; Menziani, M. C.; Cormack, A. N.; Segre, U. A New Self-Consistent Empirical Interatomic Potential Model for Oxides, Silicates and Silica-Based Glasses. *J. Phys. Chem. B* **2006**, *110*, 11780−11795.
(59) Ewald, P. P. Die Berechnung Optischer und Elektrostatischer Gitterpotentiale. *Ann. Phys.* **1921**, *369*, 253−287.
(60) Rabani, E. An Interatomic Pair Potential for Cadmium Selenide. *J. Chem. Phys.* **2002**, *116*, 258.
(61) Rabani, E. Structure and Electrostatic Properties of Passivated CdSe Nanocrystals. *J. Chem. Phys.* **2001**, *115*, 1493−1497.
(62) VandeVondele, J.; Krack, M.; Mohamed, F.; Parrinello, M.; Chassaing, T.; Hutter, J. Quickstep: Fast and Accurate Density

Functional Calculations using a Mixed Gaussian and Plane Waves Approach. *Comput. Phys. Commun.* **2005**, *167*, 103−128.
(63) Perdew, J. P.; Burke, K.; Ernzerhof, M. Generalized Gradient Approximation Made Simple. *Phys. Rev. Lett.* **1996**, *77*, 3865−3868.
(64) VandeVondele, J.; Hutter, J. Gaussian Basis Sets for Accurate Calculations on Molecular Systems in Gas and Condensed Phases. *J. Chem. Phys.* **2007**, *127*, 114105.
(65) Goedecker, S.; Teter, M.; Hutter, J. Separable Dual-Space Gaussian Pseudopotentials. *Phys. Rev. B* **1996**, *54*, 1703−1710.
(66) Adamo, C.; Barone, V. Toward Reliable Density Functional Methods without Adjustable Parameters: The PBE0 model. *J. Chem. Phys.* **1999**, *110*, 6158−6170.
(67) Guidon, M.; Hutter, J.; VandeVondele, J. Auxiliary Density Matrices Methods for Hartree-Fock Exchange Calculations. *J. Chem. Theory Comput.* **2010**, *6*, 2348−2364.

https://doi.org/10.1021/jacs.2c03039
J. Am. Chem. Soc. 2022, 144, 11296−11305